Structure of the Photochemical Reaction Path Populated via Promotion of CF_2I_2 into Its First Excited State

Patrick Z. El-Khoury,[†,●] Alexander N. Tarnovsky,[*,†] Igor Schapiro,[†,●] Mikhail N. Ryazantsev,[†] and Massimo Olivucci[*,†,‡]

Department of Chemistry and Center for Photochemical Sciences, Bowling Green State University, Bowling Green, Ohio 43403, and Universita di Siena Dipartimento di Chimica via Aldo Moro I, 53100 Siena, Italy

Received: March 30, 2009; Revised Manuscript Received: June 20, 2009

The photochemical reaction path following the promotion of CF_2I_2 into its lowest-lying excited electronic singlet state has been modeled using ab initio multiconfigurational quantum chemical calculations. It is found that a conical intersection drives the electronically excited CF_2I_2* species either to the CF_2I + I radical pair or back to the starting CF_2I_2 structure. The structures of the computed relaxation pathways explain the photoproduct selectivity previously observed in the gas phase. Furthermore, the results provide the basis for explaining the condensed-phase photochemistry of CF_2I_2.

Introduction

Acquiring a molecular-level understanding of the photochemical reactions of halogenated alkanes is essential to explaining phenomena taking place in the environment.[1−6] Besides being of practical importance, haloalkanes serve well as model systems used to explore the ultrafast phenomena following photoexcitation of small molecules in various media.[7−9] One molecule which exhibits a distinctive state-selective photochemistry is difluorodiiodomethane (CF_2I_2). This system has been thoroughly investigated in the gas phase using different experimental techniques.[10−17] The gas-phase findings following photoexcitation of CF_2I_2 with different excitation wavelengths (λ) are summarized in Scheme 1.[10−17]

SCHEME 1: Gas-Phase Results Following the Excitation of CF_2I_2 with Different Excitation Wavelengths[10−17]

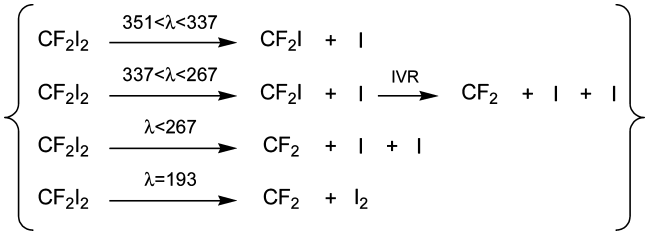

We have recently reported the formation of molecular iodine in 32% quantum yield following 350 nm excitation of CF_2I_2 in *n*-hexane.[18] This result was surprising, as the gas-phase formation of molecular iodine following the excitation of CF_2I_2 requires at least a 193 nm photon. The formation of molecular iodine was initially theorized to occur as a result of solvent mediated intramolecular vibrational energy transfer which causes the cleavage of the C−I bond of the CF_2I primary photoproduct followed by geminate combination of the two resulting iodine atoms in a solvent cage.[18] As illustrated in Scheme 1, this secondary cleavage process was not observed in gas-phase studies employing low-energy photon excitation energies in the 352−337 nm range.[15,16] In a subsequent publication,[19] ab initio MP2 calculations provided computational evidence for the existence of F_2C-I-I, an isomer of CF_2I_2 which may form as a result of primary geminate recombination of the CF_2I and I primary photoproducts in condensed phases. Unlike its structurally related H_2C-I-I analogue, the thermal stability of F_2C-I-I species is determined by the molecular elimination channel, possibly contributing to the overall yield of I_2.[19]

The recent findings mentioned above motivated the present work, where we report the photochemical reaction path following promotion of CF_2I_2 into its lowest lying excited singlet electronic state (S_1). The path is mapped using the complete active space self-consistent field (CASSCF) method.[20] The $S_0 \rightarrow S_1$ transition in CF_2I_2 is found to be an $n \rightarrow \sigma^*$ type transition. The relaxation of the electronically excited CF_2I_2* molecules from the Franck−Condon (FC) region either to a $I\cdots CF_2I$ van der Waals complex (consisting of CF_2I_2 about to break into the CF_2I + I radical pair) or back to the starting CF_2I_2 structure occurs via a conical intersection (CI) featuring an asymmetric triangular structure.

Computational Methods

The mapping of the photochemical reaction path has been mainly performed at the ab initio CASSCF level of theory with the 3-21G** basis set using Gaussian 03.[21] Below we show that the CASSCF(8,6)/3-21G** level of theory can be considered adequate for a mechanistic study. This level of theory (i) reproduces the previously reported gas-phase electron diffraction structure of CF_2I_2[22] (see Table 1S, Supporting Information), and (ii) the CF_2I_2 excited state gradient is consistent with resonance Raman data (see The Photochemical Reaction Path subsection under the Results and Discussion section of this work). The choice of active space included 8 electrons in 6 orbitals to describe decay (CF_2I_2* → CF_2I + I) expected to take place following photoexcitation of CF_2I_2 into its low lying excited electronic states.[15−17] The molecular orbitals incorporated in the active space are illustrated in Figure 1 and discussed in the Electronic Excitation subsection of the Results and Discussion section. To ascertain that the chosen approximate basis set and

* Corresponding authors. E-mail: atarnov@bgsu.edu; molivuc@bgsu.edu.
† Bowling Green State University.
‡ Universita di Siena Dipartimento di Chimica via Aldo Moro I.
● P. Z. E. and I. S. contributed equally to this work.

10.1021/jp902873h CCC: $40.75
Published on Web 08/24/2009

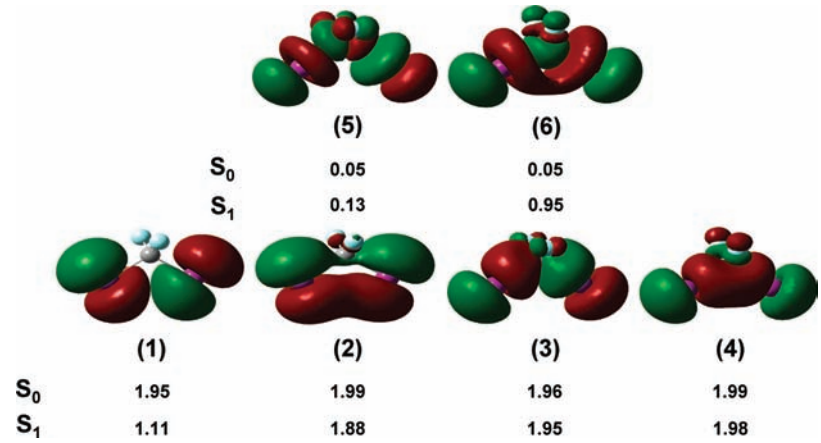

Figure 1. CASSCF/3-21G** active space molecular orbitals of CF_2I_2. These orbitals are displayed along with the values of the diagonal elements of the first-order density matrix reflecting their occupancies calculated at the CASSCF/3-21G** level of theory.

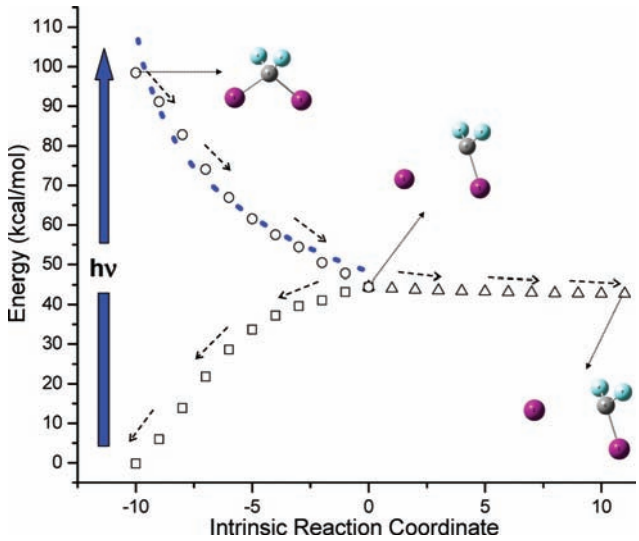

Figure 2. Photochemical reaction path (three different IRCs) showing the Franck−Condon point, the conical intersection, the I···CF_2I van der Waals complex, and the reactant, all connected by minimum energy paths (CASSCF(8,6)/3-21G**). The dotted blue line shows that the chosen approximate basis set and reduced active space do not affect the conclusions made from this work (CASSCF(12,8)/Sadlej-pVTZ).

reduced active space do not affect the conclusions made from this work, we also mapped the excited-state portion of the photochemical reaction path at the CASSCF level of theory using the Sadlej-pVTZ[23] basis set in combination with a larger active space (12 electrons in 8 orbitals). The results from these calculations are shown in Figure 2 and in Figure 1S in the Supporting Information. Notice that the analysis of the corresponding approximate and more accurate wave functions in terms of the major contributing configuration state functions indicates that the two levels of theory describe the same electronic state, as shown in Figure 2S (Supporting Information). Furthermore, and to assign the calculated electronically excited singlet state to the correct experimental spectroscopic state, the MOLCAS 7.2[24] quantum chemistry software was employed to calculate vertical transition energies at the CASSCF(12,8)/Sadlej-pVTZ//CASPT2/Sadlej-pVTZ and CASSCF(12,8)/Sadlej-pVTZ//CASPT2/Ano-RCC levels of theory.

Unconstrained geometry optimization was employed to locate the CF_2I_2 minimum on the S_0 potential energy surface. The vertical transition energy to the first singlet excited state and corresponding FC point were computed starting at the optimized S_0 minimum. A slightly distorted FC geometry was used as the starting point for the CI search and optimization between S_1 and S_0. The Moplot[25] graphical program was employed to visualize the gradient difference and derivative coupling vectors and determine the shape of the lower cone of the optimized CI (see The Photochemical Reaction Path subsection). A minimum energy path which connects the FC point to the CI was computed in terms of intrinsic reaction coordinates (IRC) using two-root state-average CASSCF gradients. Two additional IRC paths were calculated to follow the evolution of the system after $S_1 \rightarrow S_0$ decay at the CI along the S_0 single-root CASSCF potential energy surface. All IRC calculations were carried out using the methods available in Gaussian 03.[21]

Results and Discussion

1. Electronic Excitation. The molecular orbitals involved in the $S_0 \rightarrow S_1$ electronic transition of CF_2I_2 and the values of the diagonal elements of the first-order density matrices reflecting the orbital occupancies are shown in Figure 1. The transition takes place as a result of the promotion of one electron from molecular orbital (1)—occupied by two nonbonding electrons of iodine—to molecular orbital (6)—an antibonding σ^*-type orbital of the C−I bond. In S_1, the values of the diagonal elements of the first-order density matrix which reflect the occupancies of molecular orbitals (1) and (6) are 1.11 and 0.95, respectively. This finding confirms the previously reported TD-DFT random phase approximation calculations in which the first electronically excited singlet state was found to be an $n \rightarrow \sigma^*$ type transition.[26] The relative energies of different species along the calculated photochemical reaction path are given in Table 1. The calculated $S_0 \rightarrow S_1$ vertical transition energy (290 nm) at the CASSCF(8,6)/3-21G** level of theory is deceivingly consistent with the RPA-B3LYP/3-21G* (294 nm) and the maximum of the experimental steady-state absorption spectrum (~305 nm).[26] From the results shown in Table 1, it can be seen that increasing the level of theory from CASSCF(8,6)/3-21G** → CASSCF(12,8)/Sadlej-pVTZ//CASPT2/Sadlej-pVTZ → CASSCF(12,8)/Sadlej-pVTZ//CASPT2/ANO-RCC leads to the convergence of the calculated state to the first spectroscopic state located at about 349 nm and previously assigned to the first triplet state.[26] Hence, based on CASSCF//CASPT2 calculations, the first observed spectroscopic state is assigned to the first singlet excited state.

2. Photochemical Reaction Path. The photochemical reaction path following excitation of CF_2I_2 into S_1 is shown in Figure 2. An S_1/S_0 CI funnel is found to drive the electronically excited molecules (CF_2I_2*) to the primary photoproducts (CF_2I + I),

TABLE 1: Energies of the Frank−Condon Point, Conical Intersection, and I···CF_2I van der Waals Complex Relative to the Reactant (CF_2I_2) Reported at the CASSCF/3-21G Level of Theory and Compared to Previous Experimental and Theoretical Work**

species	relative energy (in nm)	relative energy (in nm)
	CASSCF(8,6)/3-21G**[a]	RPA/B3LYP/3-21G*[d]
	CASSCF(12,8)/Sadlej-pVTZ//CASPT2/Sadlej-pVTZ[b]	experimental[e]
	CASSCF(12,8)/Sadlej-pVTZ//CASPT2/ANO-RCC[c]	
CF_2I_2	-	-
CF_2I_2* (S_1 - Franck−Condon)	290[a]	n/a[d]
	336[b]	349[e], assigned to T_1
	341[c]	
CF_2I_2* (S_2 - Franck−Condon)	248[a]	294[d], assigned to S_1
	312[b]	305[e], assigned to S_1
conical intersection	642[a]	n/a
I···CF_2I van der Waals complex	674[a]	n/a

[a] This work. [b] This work. [c] This work. [d] Ref 26. [e] Ref 25, the value obtained by deconvolution of the UV-vis absorption spectrum to a sum of Gaussian functions.

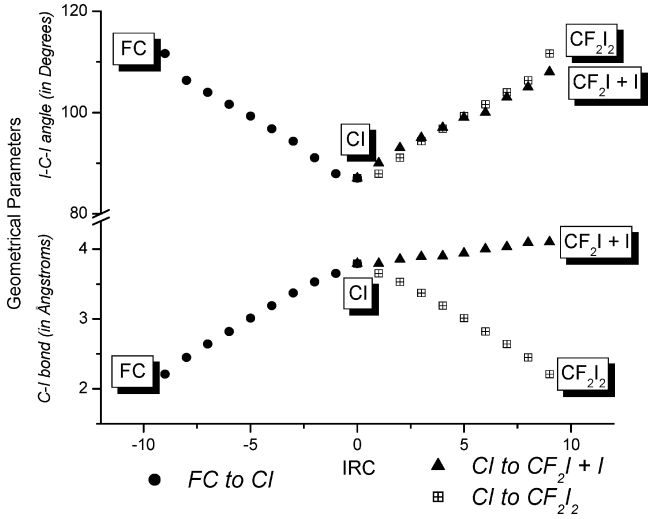

Figure 3. Change in the I−C−I (angle) and the C−I (bond) reaction coordinates along minimum energy paths on the excited-state potential energy surface (FC to CI) and on the ground state (CI to radical pair and CI to reactant).

thus explaining the selectivity experimentally observed in gas-phase studies.[15−17] In fact, the CF_2I + I radical pair is the sole product in the 352−337 nm range and the primary photoproduct in the 337−277 nm range, despite the fact that the CF_2 + I_2 is thermodynamically accessible.[15−17] It is important to note that in this work the motion out of the Franck−Condon region and toward the CI is accompanied by the lengthening of a C−I bond and a decrease in the I−C−I angle, as shown in Figure 3. This result is consistent with resonance Raman spectra recorded following 341.5 nm excitation of CF_2I_2 in solution[26,27] where an enhancement of the I−C−I asymmetric stretch and the I−C−I bend modes was reported.

A scan along a circular cross-section centered at the CI and spanning the branching plane (the plane formed by the gradient difference and derivative coupling vectors illustrated in Figure 5A) has been generated using the Moplot graphical interface program.[25] Single-point CASSCF(8,6)/3-21G** calculations were performed to determine the S_0 energy profile along the scan (Figure 4). At a trust radius of 0.4 Å, two reaction channels (channels A and B) were found at a radial distance of about 180 degrees. Two IRCs starting from the CI and directed along the latter-mentioned two cross-section energy minima were computed and demonstrate that the channels lead toward the CF_2I + I photoproduct and the CF_2I_2 initial reactant, respectively. The changes in electronic wave function along the circular cross-section are also monitored by plotting the occupancies of molecular orbitals 1 and 6 extracted from the diagonal elements of the first-order density matrices (see the bottom right of Figure 4). At an angle of 100 degrees (corresponding to channel A), the electronic configuration structure of molecular orbitals 1 (doubly occupied) and 6 (empty) reflects the ground-state electronic configuration, providing an additional proof that channel A leads to CF_2I_2. On the other hand, the occupancies of molecular orbitals 1 and 6 (both singly occupied) at a displacement angle of about 280 degrees (corresponding to channel B) reflect the electronic configuration of the excited state potential, hinting that the reaction points diabatically toward the CF_2I + I radical pair. At this stage, a branching diagram[28] which describes the chemical character of the CI along the gradient difference and derivative coupling vectors can be plotted (Figure 5). The X and X_{-1} directions represent the reactive channels where the reaction evolves along the gradient difference vector to yield the CF_2I + I radical pair in the positive direction and the CF_2I_2 reactant in the opposite direction. The geometries resulting from displacing the CI structure along the derivative coupling vector in the Y_{-1} direction and Y direction consistently suggest that these displacements are nonreactive. These directions correspond to displacements that create unstable electronic structures (indeed, these correspond to the maxima of the circular cross-section on the energy profile). In valence-bond terms in the Y direction, one has a repulsive situation thus pointing to a relaxation toward the CF_2I + I radical pair. In contrast, along the Y_{-1} direction, one has a bonding situation thus pointing the system toward the reactant.

The progression from the CI both to the CF_2I + I radical pair and the reactant (CF_2I_2) on the ground-state potential energy surface is described by plotting the C−I and I−C−I coordinates along the two IRCs, as illustrated in Figure 3. From the conical intersection structure, an increase in both the I−C−I angle and the C−I bond length leads to the CF_2I + I radical pair, whereas an increase in the I−C−I angle simultaneously with a decrease in the C−I bond length leads back to the starting CF_2I_2 structure. Thus, the sole primary photoproducts expected to form following the promotion of CF_2I_2 to the first electronically excited state are the CF_2I + I species. This result is consistent with previous gas-phase experiments,[15,16] and resonance Raman data.[26,27] Our condensed-phase findings[18,19] highlighted below can also be rationalized using this result.

3. Extrapolation to Liquid-Phase Results. As a result of the presence of a CI, a few extrapolations can be drawn about excitation of CF_2I_2 into S_1 in solution. Since the calculated

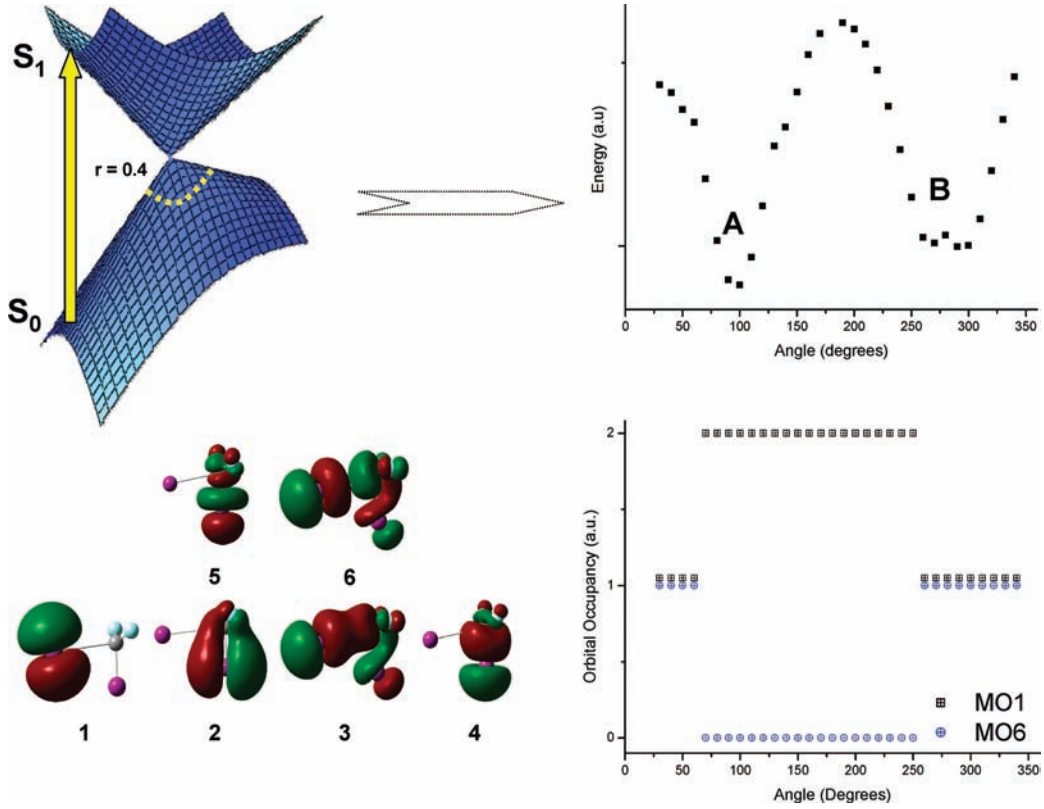

Figure 4. Upper left part: a schematic diagram of the photochemical funnel. Lower left part: the molecular orbitals at the conical intersection geometry. Relative energies and change in electronic wave function (the occupancies of MOs 1 and 6) as a function of angular displacement from the CI at a trust radius of 0.4 Å for several geometries tracing the lower cone of the CI are plotted in the right part of the figure. Right part: the topography and orbital occupancies of the lower CI cone.

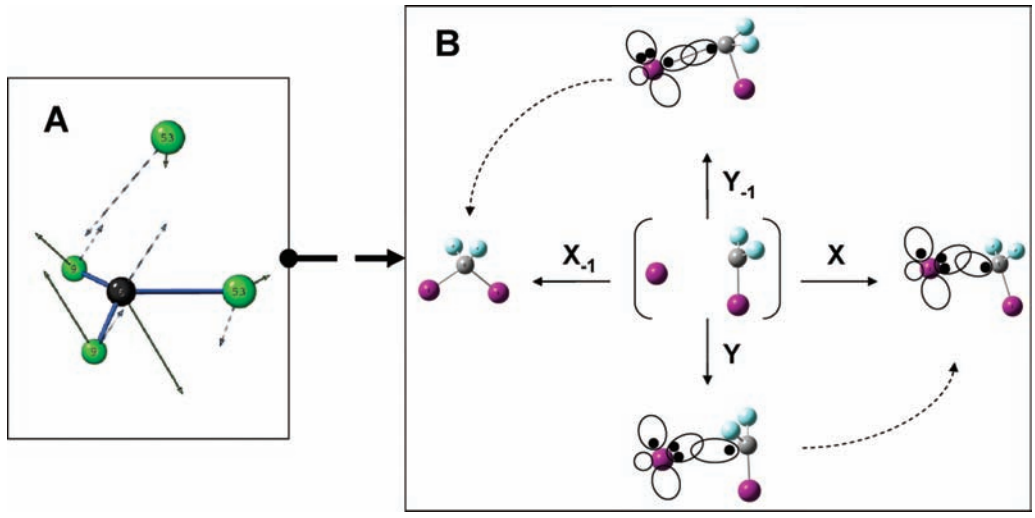

Figure 5. Panel A, the conical intersection geometry along with the computed gradient difference (dotted line) and derivative coupling (solid line) vectors are plotted. The gradient difference and derivative coupling vectors are orthogonalized. A branching diagram describing the progress of the photochemical reaction through the CI following displacement of the CI along the reactive gradient difference (X and X_{-1}) and the nonreactive derivative coupling (Y and Y_{-1}) vectors is shown in Panel B. A valence bond interpretation (predominating resonance formula) of the process is also schematically represented in Panel B.

excited state is found to be repulsive in this work and a typical excited-state lifetime is on the order of ~75 fs for low-lying electronic excited state(s) in CF_2I_2,[18] the presence of weakly interacting molecular liquid solvents is not expected to affect the topography of the excited state[29−31] and hence the passage of excited CF_2I_2* through the CI to CF_2I + I. After the primary radical pair photoproduct forms, the presence of the solvent cage as a physical boundary arrests their mutual separation. Inside the solvent cage, the ground state chemistry leading to molecular iodine formation then takes place. The latter may occur as a result of (a) the recombination of the CF_2I and I primary photoproducts to form F_2C-I-I, eventually leading to the formation of I_2 through C−I bond cleavage in this isomer species,[19] and (b) a solvent-mediated intramolecular vibrational energy transfer resulting in the cleavage of a second iodine atom from the vibrationally hot CF_2I photoproduct followed by primary geminate combination of the two iodine fragments in a solvent cage.[18] The sequential

SCHEME 2: Generalized Reaction Mechanism Which Accounts for the Formation of Molecular Iodine upon 350 nm Excitation of CF_2I_2 in Solution

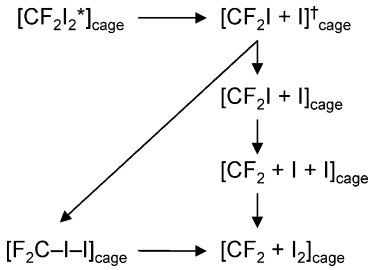

three-body mechanism (b) was not reported to be a major photodissociation pathway in gas-phase experiments which employ low excitation energies in the 352−337 nm range but is accessible at higher excitation energies in the 337−267 nm range.[15,16]

Conclusions

The photochemical reaction path following the promotion of CF_2I_2 into its lowest lying electronically excited singlet state is mapped at the CASSCF(8,6)/3-21G** level of theory. We find that: (i) coordinates other than the carbon−halogen repulsive bond-breaking coordinate are involved (for example, I−C−I bending motion) and (ii) the excited state species are "funneled" to the ground-state potential energy surface through a conical intersection. Moreover, as a result of the presence of a conical intersection and the topology of the first electronically excited state, a few conclusions about the condensed-phase photochemistry are drawn. A generalized reaction scheme is shown in Scheme 2.[18,19] A valid approximation is the excited-state topography from the Franck−Condon point to the CI not being greatly affected by the presence of weakly interacting molecular liquids.[29−31] Thus, the formation of molecular iodine from CF_2I_2* in solution is a ground-state process which either proceeds though (a) a precursor (F_2C−I−I) which breaks to form CF_2 + I_2 and/or (b) as a result of solvent mediated intramolecular vibrational energy transfer which leads to the cleavage of a second iodine atom from vibrationally hot CF_2I followed by the subsequent combination of two iodine fragments in the solvent cage to form CF_2 + I_2. We are currently conducting experiments which aim to distinguish between mechanisms (a) and (b).

Acknowledgment. This work is supported by the National Science Foundation under CHE-0847707 (CAREER, ANT). M.O. is grateful to the Center for Photochemical Sciences at Bowling Green State University for a startup grant. This work was also supported in part by an allocation of computing time from the Ohio Supercomputer Center.

Supporting Information Available: Table 1S and Figures 1S and 2S. This material is available free of charge via the Internet at http://pubs.acs.org.

References and Notes

(1) Teh, Y. A.; Mazeas, O.; Atwood, A. R.; Abel, T.; Rhew, R. C. *Global Change Biol.* **2009**, *15*, 330–345.

(2) Wishkerman, A.; Gebhardt, S.; McRoberts, C. W.; Hamilton, J. T. G.; Williams, J.; Keppler, F. *Environ. Sci. Technol.* **2008**, *42*, 6837–6842.

(3) Richardson, S. D.; Fasano, F.; Ellington, J. J.; Crumley, F. G.; Buettner, K. M.; Evans, J. J.; Blount, B. C.; Silva, L. K.; Waite, T. J.; Luther, G. W.; McKague, A. B.; Miltner, R. J.; Wagner, E. D.; Plewa, M. J. *Environ. Sci. Technol.* **2008**, *42*, 8330–8338.

(4) Rhew, R. C.; Miller, B. R.; Weiss, R. F. *Atmos. Environ.* **2008**, *42*, 7135–7140.

(5) Mead, M. I.; White, L. R.; Nickless, G.; Wang, K. Y.; Shallcross, D. E. *Atmos. Environ.* **2008**, *42*, 337–345.

(6) Rhew, R. C.; Abel, T. *Environ. Sci. Technol.* **2007**, *41*, 7837–7843.

(7) Brixner, T.; Gerber, G. *ChemPhysChem* **2003**, *4*, 418–438.

(8) Clary, D. C. *Science* **1998**, *279*, 1879–1882.

(9) Cain, S. R.; Hoffmann, R.; Grant, E. R. *J. Phys. Chem.* **1981**, *85*, 4046–4051.

(10) Roeterdink, W. G.; Janssen, M. H. M. *J. Chem. Phys.* **2002**, *117*, 6500–6510.

(11) Scheld, H. A.; Furlan, A.; Huber, J. R. *Chem. Phys. Lett.* **2000**, *326*, 366–374.

(12) Farmanara, P.; Stert, V.; Ritze, H. H.; Radloff, W. *J. Chem. Phys.* **2000**, *113*, 1705–1713.

(13) Radloff, W.; Farmanara, P.; Stert, V.; Schreiber, E.; Huber, J. R. *Chem. Phys. Lett.* **1998**, *291*, 173–178.

(14) Cao, J.; Ihee, H.; Zewail, A. H. *Chem. Phys. Lett.* **1998**, *290*, 1–8.

(15) Bergmann, K.; Carter, R. T.; Hall, G. E.; Huber, J. R. *J. Chem. Phys.* **1998**, *109*, 474–483.

(16) Baum, G.; Felder, P.; Huber, J. R. *J. Chem. Phys.* **1993**, *98*, 1999–2010.

(17) Wannenmacher, E. A. J.; Felder, P.; Huber, J. R. *J. Chem. Phys.* **1991**, *95*, 986–997.

(18) El-Khoury, P. Z.; Tarnovsky, A. N. *Chem. Phys. Lett.* **2008**, *453*, 160–166.

(19) El-Khoury, P. Z.; Olivucci, M.; Tarnovsky, A. N. *Chem. Phys. Lett.* **2008**, *462*, 192–195.

(20) Roos, B. O.; Taylor, P. R. *Chem. Phys.* **1980**, *48*, 157–173.

(21) Frisch, M. J. *GAUSSIAN 03*, Revision C02; Gaussian Inc.: Pittsburgh, PA, 2003.

(22) Mack, H. G.; Oberhammer, H.; John, E. O.; Kirchmeier, R. L.; Shreeve, J. M. *J. Mol. Struct.* **1991**, *250*, 103–106.

(23) Sadlej, A. J. *Theor. Chim. Acta* **1992**, *81*, 339–354.

(24) Karlstrom, G.; Lindh, R.; Malmqvist, P. A.; Roos, B. O.; Ryde, U.; Veryazov, V.; Widmark, P. O.; Cossi, M.; Schimmelpfennig, B.; Neogrady, P.; Seijo, L. *Elsevier Science Bv*; 2003; p222−239.

(25) Olkhov, R. V.; Matzinger, S.; Bally, T. *MoPlot (Molecular Orbital Plotting program)*, version 1.85 for Windows, Linux and MacOS X; University of Fribourg: Switzerland, 2005. See: http://www-chem-unifr.ch/tb/moplot/moplot.html.

(26) Zheng, X. M.; Phillips, D. L. *Chem. Phys. Lett.* **2000**, *316*, 524–530.

(27) Zheng, X. M.; Phillips, D. L. *Chem. Phys. Lett.* **1999**, *313*, 467–472.

(28) Migani, A.; Olivucci, M. Conical Intersections and Organic Reaction Mechanisms. In *Conical Intersections: Electronic Structure, Dynamics and Spectroscopy*; Domcke, W., Yarkony, D., Kö ppel, H., Eds.; World Scientific: River Edge, NJ, 2004; Vol. 15.

(29) Levine, B. G.; Martinez, T. J. *Annu. Rev. Phys. Chem.* **2007**, *58*, 613–634.

(30) Spezia, R.; Burghardt, I.; Hynes, J. T. *Mol. Phys.* **2006**, *104*, 903–914.

(31) Burghardt, I.; Cederbaum, L. S.; Hynes, J. T. *Faraday Discuss.* **2004**, 395–411.

JP902873H